NASA
Technical
Paper
2013

June 1982

Performance Characteristics of Axisymmetric Convergent-Divergent Exhaust Nozzles With Longitudinal Slots in the Divergent Flaps

Laurence D. Leavitt
and Linda S. Bangert

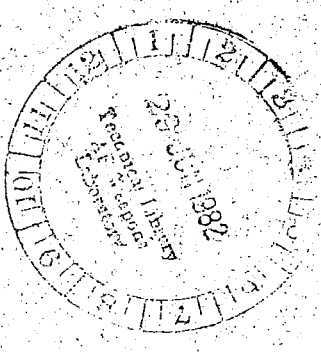

NASA

NASA Technical Paper 2013

1982

Performance Characteristics of Axisymmetric Convergent-Divergent Exhaust Nozzles With Longitudinal Slots in the Divergent Flaps

Laurence D. Leavitt
and Linda S. Bangert
Langley Research Center
Hampton, Virginia

National Aeronautics
and Space Administration

Scientific and Technical Information Branch

INTRODUCTION

Multimission aircraft capable of operating over a broad range of Mach numbers, altitudes, and angles of attack have been emphasized in recent years. These multimission aircraft typically require a variable geometry nozzle to provide high nozzle internal (thrust) performance over the range of operating Mach numbers and nozzle pressure ratios. The next generation of fighter aircraft may require the ability to land on short or bomb damaged runways, which will probably mean adding thrust-reversing capability to the aircraft design. Considerable research has been conducted on both axisymmetric and nonaxisymmetric nozzle configurations with thrust-reversing capability (see refs. 1 and 2). If a downstream (from nozzle throat) reverser concept is used, where nozzle divergent flaps are used as flow diverters (ref. 2), special consideration must be given to the mechanization of the nozzle/reverser combination and its impact on nozzle geometry at flight conditions other than landing. The use of a light-weight downstream reverser concept in intermediate and maximum afterburning forward-flight modes may result in the slotting (ventilation) of the nozzle divergent flaps.

Since the ventilation effects of the divergent flaps on axisymmetric nozzle performance were unknown, except for the work reported in reference 3, an investigation was conducted in the Langley 16-Foot Transonic Tunnel and in the static-test facility of that tunnel to determine these effects. Tests were conducted at 0° angle of attack at static conditions and at free-stream Mach numbers from 0.6 to 1.2. The ratio of jet total pressure to free-stream static pressure (nozzle pressure ratio) was varied from 1.0 (jet off) to approximately 14.0 depending upon Mach number.

SYMBOLS

A_e	nozzle exit area, cm^2
A_{max}	maximum cross-sectional area of model, 182.415 cm^2
A_{seal}	internal-cavity cross-sectional area of model, cm^2
A_t	nozzle geometric throat area, cm^2
$D_{f,cb}$	friction drag on model centerbody, N
D_n	nozzle drag, N
d_{max}	maximum model diameter, 15.24 cm
F	nozzle gross thrust, N
$F_{A,bal}$	axial force measured by balance (positive forward), N
$F_{A,mom}$	momentum tare axial force due to bellows, N

F_i ideal isentropic gross thrust, N

ι nozzle divergent flap length, cm

M free-stream Mach number

p local static pressure, Pa

p_a ambient pressure, Pa

p_{es} external static pressure at metric break, Pa

p_i internal static pressure, Pa

$p_{t,j}$ jet total pressure, Pa

p_∞ free-stream static pressure, Pa

x axial distance from nozzle throat (positive downstream), cm

φ meridian angle about model axis (positive for clockwise direction when facing upstream), 0° at top of model, deg

Abbreviations:

B baseline

Sta. station

STF static-test facility

V ventilated

16TT 16-Foot Transonic Tunnel

APPARATUS AND METHODS

Test Facilities

This experimental investigation was conducted in the Langley 16-Foot Transonic Tunnel and in the static-test facility of that tunnel. The 16-Foot Transonic Tunnel (16TT) is a single-return, atmospheric tunnel with a slotted, octagonal test section and continuous air exchange. The tunnel has a Mach number range capability from M = 0.20 to M = 1.30. A complete description of the 16-Foot Transonic Tunnel can be found in reference 4. Testing in the static-test facility is done in a room with a high ceiling where the jet exhausts to the atmosphere through a large open doorway. The control room is remotely located from the test area. This facility utilizes the same clean, dry-air supply as that used in the 16-Foot Transonic Tunnel and a similar air-control system, including valving, filters, and a heat exchanger (to operate the jet flow at constant stagnation temperature). Photographs of model installations in the 16TT and the static-test facility are shown in figures 1(a) and 1(b).

Single-Engine Propulsion Simulation System

A sketch of the single-engine air-powered nacelle model on which various nozzles were mounted is presented in figure 2 with a typical nozzle configuration attached. An external high-pressure air system provided a continuous flow of clean, dry air at a controlled temperature of about 300 K. This high-pressure air was varied up to approximately 14 atm (1 atm = 101.3 kPa) and was brought through the support strut by six tubes which connect to a high-pressure plenum chamber. As shown in figure 2, the air was then discharged perpendicularly into the model low-pressure plenum through eight multiholed sonic nozzles equally spaced around the high-pressure plenum. This method was designed to minimize any forces imposed by the transfer of axial momentum as the air is passed from the nonmetric (not mounted on the force balance) high-pressure plenum to the metric low-pressure plenum. Two flexible metal bellows are used as seals and serve to compensate for axial forces caused by pressurization. The air was then passed from the model low-pressure plenum through a transition section, choke plate, and instrumentation section which were common for all nozzles investigated. All nozzle configurations were attached to the instrumentation section at model station 127.00.

Nozzle Design

The baseline nozzle configuration simulated a variable-geometry, balanced-beam, convergent-divergent conical nozzle typical of those currently in use on modern fighter aircraft, but designed with a higher expansion-ratio capability and with longer divergent-flap lengths. The nozzle throat area of all nozzles tested represented maximum nonaugmented (dry power) nozzle operation. Sketches of the three baseline configurations are shown in figures 3(a), 3(b), and 3(c). Nozzle configurations B-1.22 (baseline nozzle, $A_e/A_t = 1.22$) and B-2.24 (figs. 3(a) and 3(b), respectively) were previously tested and the results are reported in reference 5 as configurations D-1.22-L and D-2.24-L, respectively. The intermediate-expansion-ratio baseline nozzle B-1.91 (fig. 3(c)) was made by simply removing the shroud from configuration B-2.24, thereby reducing the divergent-flap length and nozzle expansion ratio. Note, however, that this configuration and the corresponding ventilated configuration (V-1.91) were only tested at static conditions as the external geometries were not realistic for wind-on tests.

The ventilated nozzle configurations shown in figures 3(d), 3(e), and 3(f) and in figures 1(c) and 1(d) were designed to simulate an axisymmetric nozzle incorporating a three-door thrust-reverser concept (ref. 2). In the dry-power, subsonic (low A_e/A_t), forward-flight mode, the axisymmetric thrust-reverser geometry is that of a typical convergent-divergent nozzle (baseline nozzle). However, as expansion ratio (A_e/A_t) is increased to allow fully expanded flow at higher Mach numbers, V-shaped slots appear as the divergent flaps are actuated (see figs. 1(d), 3(e), and 3(f)). The changing of the throat area to the maximum afterburning mode results in trapezoidal shaped slots similar to those shown in figures 1(c) and 3(d). Since existing nozzle hardware was used, an exact simulation of the geometry for the actual axisymmetric thrust-reverser nozzle concept (throat area, expansion ratio, flap length, etc.) was not possible. Hence, the determination of nozzle performance increments between baseline and slotted nozzles was the primary objective of the investigation. It should be noted that the slot dimensions presented in figures 3(d), 3(e), and 3(f) represent nominal values.

Instrumentation

A three-component strain-gage balance was used to measure forces and moments on the model downstream of station 67.31 (see fig. 2). Jet total pressure was measured at a fixed station in the instrumentation section by means of a five-probe rake and a single probe (not shown). A thermocouple, also located in the instrumentation section, was used to measure jet total temperature. The total pressure and temperature of the air in the high-pressure plenum were measured before the airflow was discharged through the eight sonic nozzles into the centerbody. These measurements were used in calculating the nozzle mass flow rate as explained in reference 6.

Internal pressures were measured in the forebody cavity at two orifice locations. Pressure in the metric gap (Sta. 67.31) was measured at four orifice locations in the forebody gap base. The ventilated nozzle configurations contained internal nozzle static-pressure orifices. These orifices were arranged in two rows on the nozzle divergent flaps with one row (row 1) located halfway between the slots and the other row (row 2) located parallel with and 0.635 cm from the slot edge. Locations of these orifices are given in figures 3(d), 3(e), and 3(f). The baseline nozzle configurations did not contain internal nozzle static-pressure instrumentation.

Tests

Data were obtained in the static-test facility at static conditions ($M = 0$), and in the Langley 16-Foot Transonic Tunnel at static conditions and at Mach numbers from 0.60 to 1.20. Angle of attack was held constant at 0° during the investigation. The ratio of jet total pressure to free-stream static pressure (or p_a at $M = 0$) was varied from 1.0 (jet off) to approximately 14.0 depending on Mach number. To insure a turbulent boundary layer over the external nozzle surfaces, a 0.38-cm-wide transition strip of No. 100 carborundum grit was fixed 5.72 cm downstream of the model nose for all wind-on tests.

Data Reduction

All data were recorded simultaneously on magnetic tape. At each test point, 50 frames of data were recorded at a rate of 10 frames per second. The samples were averaged, and the averaged values were used for computations. At wind-on conditions, thrust-minus-nozzle drag was obtained from the five-component balance and computed from the following equation:

$$F - D_n = F_{A,bal} + (p_{es} - p_\infty)(A_{max} - A_{seal}) + (p_i - p_\infty)A_{seal} - F_{A,mom} + D_{f,cb} \qquad (1)$$

Included in the balance term $F_{A,bal}$ are internal and external axial forces on the metric centerbody and nozzle, including thrust, nozzle drag (friction and pressure), centerbody friction drag (pressure drag equal to zero since the centerbody has no projected area), axial force resulting from a pressure-area term acting at the metric break, and bellows momentum tares. The second and third terms of equation (1) correct the balance measurement for pressure-area forces acting at the metric break. These terms arise from the fact that the model is a partially metric, afterbody propulsion model. These terms would not exist for typical aerodynamic studies of completely metric (no metric break) models. The fourth term of equation (1) corrects

the balance measurement for bellows momentum tares. Although the bellows arrangement was designed to minimize pressure and momentum interactions with the balance, small bellows tares on axial force still exist. These tares result from a small pressure difference between the ends of the bellows when internal velocities are high and also from small differences in the forward and aft bellows spring constants when the bellows are pressurized. Bellows tares were determined by testing calibration nozzles with known performances; more detailed discussion of this procedure is contained in references 6 and 7. The last term of equation (1) removes the friction drag of the cylindrical centerbody (Sta. 67.31 to Sta. 137.16) from the balance measurement. Friction drag of the centerbody was removed from all performance parameters since this part of the model is not actually part of the nozzle design. Friction drag was calculated using the Frankl and Voishel equation for compressible, turbulent flow on a flat plate as given in reference 8. At static ($M = 0$) conditions, the second, third, and last terms drop out and $F_{A,bal}$ includes only internal axial forces on nozzle (thrust) and bellows momentum tares.

The basic performance parameter used in evaluating static internal performance is the ratio of measured thrust to the ideal isentropic thrust F/F_i. At wind-on conditions, the thrust-minus-drag ratio $(F - D_n)/F_i$ is used in evaluating performance.

RESULTS AND DISCUSSION

Internal Static-Pressure Distributions

Internal static-pressure data for the three ventilated (slotted) nozzles are presented in figures 4 to 6 at $M = 0$. Part (a) of each figure presents data for the center-line row (row 1) of static-pressure orifices and part (b) of each figure presents data for the static-pressure orifices parallel to the slot edge (row 2). Since the baseline nozzles had no internal static-pressure instrumentation, a two-dimensional, inviscid, time-dependent computer code called NAP (ref. 9) was used to compute the internal pressure distribution at fully-expanded-flow conditions (computation at design nozzle pressure ratios, 4.0, 9.8, and 13.0 for B-1.22, B-1.91, and B-2.24, respectively) for each baseline nozzle. These analytical results are included in part (a) of figures 4 to 6 and were used as a basis for comparison of baseline and ventilated (or slotted) pressure distributions.

As a result of the large nozzle throat areas tested, a limited nozzle pressure ratio capability existed (maximum $p_{t,j}/p_a = 7.0$ at $M = 0$). Because of model balance and airflow system restrictions, it was not possible to test the $A_e/A_t = 1.91$ and $A_e/A_t = 2.24$ configurations at or above their design nozzle pressure ratios (9.8 and 13.0, respectively) at static conditions. Thus, a large portion of the internal pressure data were obtained during overexpanded nozzle operation and indicate large regions of exhaust-flow separation from the nozzle divergent flaps. Comparisons of row 1 and row 2 pressure data (parts (a) and (b), respectively, of figs. 4 to 6) indicate that the regions of separation generally became more extensive near the slot, as expected. This observation is similar to those made in references 10 and 11 concerning nonaxisymmetric nozzle sidewall cutback and the increased exhaust-flow separation from the divergent flaps near the sidewall region.

Comparison of ventilated nozzle pressure distributions for configuration V-1.22 (fig. 4(a)) with the NAP computation (assumed to be representative of the nonventilated or baseline configuration B-1.22 operating fully expanded) indicates that ventilating the nozzle divergent flaps significantly reduced static pressures through-

out the nozzle when the nozzle is operating near design or underexpanded ($p_{t,j}/p_a > 4.0$). This reduction in static pressure is similar to the effect observed when the nozzle expansion ratio A_e/A_t is increased. A similar trend is not indicated by the static-pressure distributions of the high- and intermediate-expansion-ratio nozzles found in figures 5(a) and 6(a), respectively. In fact, the unseparated ventilated nozzle data (e.g., $p_{t,j}/p_\infty = 7.0$) and the fully expanded baseline NAP code data agree very well. It can only be assumed that the large trapezoidal ventilation slots (of configuration V-1.22) which began just aft of the nozzle throat, resulted in a large portion of the exhaust flow being expanded through the slots, particularly during underexpanded nozzle operation. The effects of ventilation are not all adverse as will be seen in the discussion of static and wind-on nozzle performance.

Static Internal Performance

Since the present investigation was conducted in both the 16-Foot Transonic Wind Tunnel and the static-test facility of that tunnel, and two of the baseline nozzles were tested in an earlier investigation (ref. 5), some indication of data repeatability seemed warranted. Figure 7 presents a comparison of static (M = 0) thrust ratios for the baseline nozzles of the present investigation with the same nozzle configurations as reported in reference 5. As can be seen, repeatability was generally within 0.5 percent. In addition, the ventilated nozzle configurations V-1.22 and V-2.24 were tested in both the static-test facility and the 16-Foot Transonic Tunnel at static conditions. These data are shown in figures 8(a) and 8(b) and again repeatability was generally within 0.5 percent. This repeatability allows direct comparison of data from both facilities of the present investigation with data of the previous investigation (ref. 5).

Comparisons of baseline and ventilated nozzle internal performance are presented in figure 8. As seen in figure 8(a), ventilation had an extremely large effect on performance for the low-expansion-ratio nozzle. For nozzle pressure ratios less than 3.0 the slotted nozzle provided the best performance. Above $p_{t,j}/p_a = 3.0$, the baseline nozzle was significantly better. The more important observation, however, is the general nature of the curves. The baseline nozzle internal performance is typical of a convergent-divergent nozzle with peak performance being obtained near the design nozzle pressure ratio of 4.0. The ventilated nozzle performance is more typical of a convergent nozzle or extremely low-expansion-ratio ($A_e/A_t < 1.04$) nozzle, with peak performance occurring between a nozzle pressure ratio of 2.0 and 2.5. Unfortunately, this trend seems to be in direct conflict with the pressure distribution data (see fig. 4(a)), which indicates an increased expansion on the divergent flaps at nozzle pressure ratios greater than 3.0 for this configuration. However, as stated previously, the extremely large trapezoidal slots may have resulted in a large portion of the nozzle exhaust flow being expanded through the slots (less efficiently). In addition to the losses, at $p_{t,j}/p_a > 3.0$ it can be seen in figure 8(a) that there is a net loss in peak performance of approximately 0.5 percent for the ventilated nozzle.

Thrust ratio comparisons of the high- and intermediate-expansion-ratio baseline and ventilated nozzles (figs. 8(b) and 8(c)) also show significant improvements in overexpanded nozzle performance. The reduction in overexpansion losses is thought to be at least partially due to the ability of the slots to relieve some of the adverse effects of the separated exhaust flow on the internal surface (divergent flaps). Since design nozzle pressure ratios could not be reached at static (M = 0) condi-

tions, it is not known what effects, if any, ventilation has on underexpanded and peak nozzle performance of these two nozzles.

Wind-On Nozzle Performance

Variation of thrust-minus-drag ratio with nozzle pressure ratio at several test Mach numbers is presented in figure 9 for both the low- and high-expansion-ratio nozzles (figs. 9(a) and 9(b), respectively). Comparisons of the baseline and ventilated nozzles are made. The baseline nozzle data were obtained in a previous investigation and are reported in reference 5.

In general, internal static pressure at a given nozzle pressure ratio decreased as Mach number increased. As a result, peak internal performance of these nozzles occurred at increasingly higher nozzle pressure ratios as Mach number increased. In addition, at a given value of $p_{t,j}/p_\infty$ drag becomes a higher percentage of $(F - D_n)/F_i$ as M increases, thus it requires a higher nozzle pressure ratio to reach the same level of $(F - D_n)/F_i$. The thrust-minus-drag ratios shown in figure 9 indicate that for the baseline nozzle, peak performance generally decreased as Mach number increased. This is a direct result of increased boattail drag with increasing Mach number, as reported in reference 5. This observation is most evident with the low-expansion-ratio (high nozzle boattail angle) nozzle data (fig. 9(a)). Examination of the ventilated nozzle data indicates that the level of peak performance did not necessarily decrease with increasing M. In fact, for configuration V-1.22, the highest thrust-minus-drag performance occurred at $M = 0.8$. Trends of the V-2.24 data (fig. 9(b)) indicate that peak thrust-minus-drag performance would either remain the same or increase as Mach number increases (even though peak performance was only attained at $M = 0.95$ and 1.2).

Comparison of baseline and ventilated nozzle configurations indicates trends similar to the static results. Thrust-minus-drag ratio for the ventilated nozzles was higher at the lower nozzle pressure ratios and lower at the higher nozzle pressure ratios when compared with the baseline nozzles. It is also evident that the ventilated nozzles have a peak wind-on performance level which is generally lower than the baseline nozzles. The performance increments between baseline and ventilated nozzles were, in general, smaller at $M = 1.2$.

CONCLUSIONS

An investigation has been conducted in the Langley 16-Foot Transonic Tunnel and in the static-test facility of that tunnel to determine the effects of divergent flap ventilation of an axisymmetric nozzle on nozzle internal (static) and wind-on performance. Tests were conducted at 0° angle of attack at static conditions and at Mach numbers from 0.6 to 1.2. Ratios of jet total pressure to free-stream static pressure were varied from 1.0 (jet off) to approximately 14.0 depending on Mach number. Results of the investigation indicate the following conclusions:

1. Ventilation of the nozzles increased the amount of flow separation on the internal divergent flap.

2. Nozzle divergent-flap ventilation acted to reduce peak internal and thrust-minus-drag performance.

3. Ventilation generally provided large performance benefits at overexpanded conditions and performance reductions at underexpanded conditions when compared to the baseline nozzles. Performance improvements at nozzle pressure ratios below design pressure ratios (overexpanded) are believed to result from the ability of the slot to relieve some of the adverse effects of the separated exhaust flow on the internal surface.

Langley Research Center
National Aeronautics and Space Administration
Hampton, VA 23665
April 13, 1982

REFERENCES

1. Capone, Francis J.: The Nonaxisymmetric Nozzle - It is for Real. AIAA Paper 79-1810, Aug. 1979.

2. Blackman, J. P.; and Eigenmann, M. F.: Axisymmetric Approach and Landing Thrust Reversers. AIAA-81-1650, Aug. 1981.

3. Runckel, Jack F.: Preliminary Transonic Performance Results for Solid and Slotted Turbojet Nacelle Afterbodies Incorporating Fixed Divergent Jet Nozzles Designed for Supersonic Operation. NASA MEMO 10-24-58L, 1958.

4. Corson, Blake W., Jr.; Runckel, Jack F.; and Igoe, William B.: Calibration of the Langley 16-Foot Transonic Tunnel With Test Section Air Removal. NASA TR R-423, 1974.

5. Berrier, Bobby L.; and Re, Richard J.: Investigation of Convergent-Divergent Nozzles Applicable to Reduced-Power Supersonic Cruise Aircraft. NASA TP-1766, 1980.

6. Capone, Francis J.: Static Performance of Five Twin-Engine Nonaxisymmetric Nozzles With Vectoring and Reversing Capability. NASA TP-1224, 1978.

7. Capone, Francis J.: The Effects on Propulsion-Induced Aerodynamic Forces of Vectoring a Partial-Span Rectangular Jet at Mach Numbers From 0.40 to 1.20. NASA TN D-8039, 1975.

8. Shapiro, Ascher H.: The Dynamics and Thermodynamics of Compressible Fluid Flow. Vol. II. Ronald Press Co., c.1954.

9. Cline, Michael C.: NAP: A Computer Program for the Computation of Two-Dimensional, Time-Dependent, Inviscid Nozzle Flow. LA-5984 (Contract W-7405-ENG. 36), Los Alamos Sci. Lab., Univ. of California, Jan. 1977.

10. Berrier, Bobby L.; and Re, Richard J.: Effect of Several Geometric Parameters on the Static Internal Performance of Three Nonaxisymmetric Nozzle Concepts. NASA TP-1468, 1979.

11. Yetter, Jeffery A.; and Leavitt, Laurence D.: Effects of Sidewall Geometry on the Installed Performance of Nonaxisymmetric Convergent-Divergent Exhaust Nozzles. NASA TP-1771, 1980.

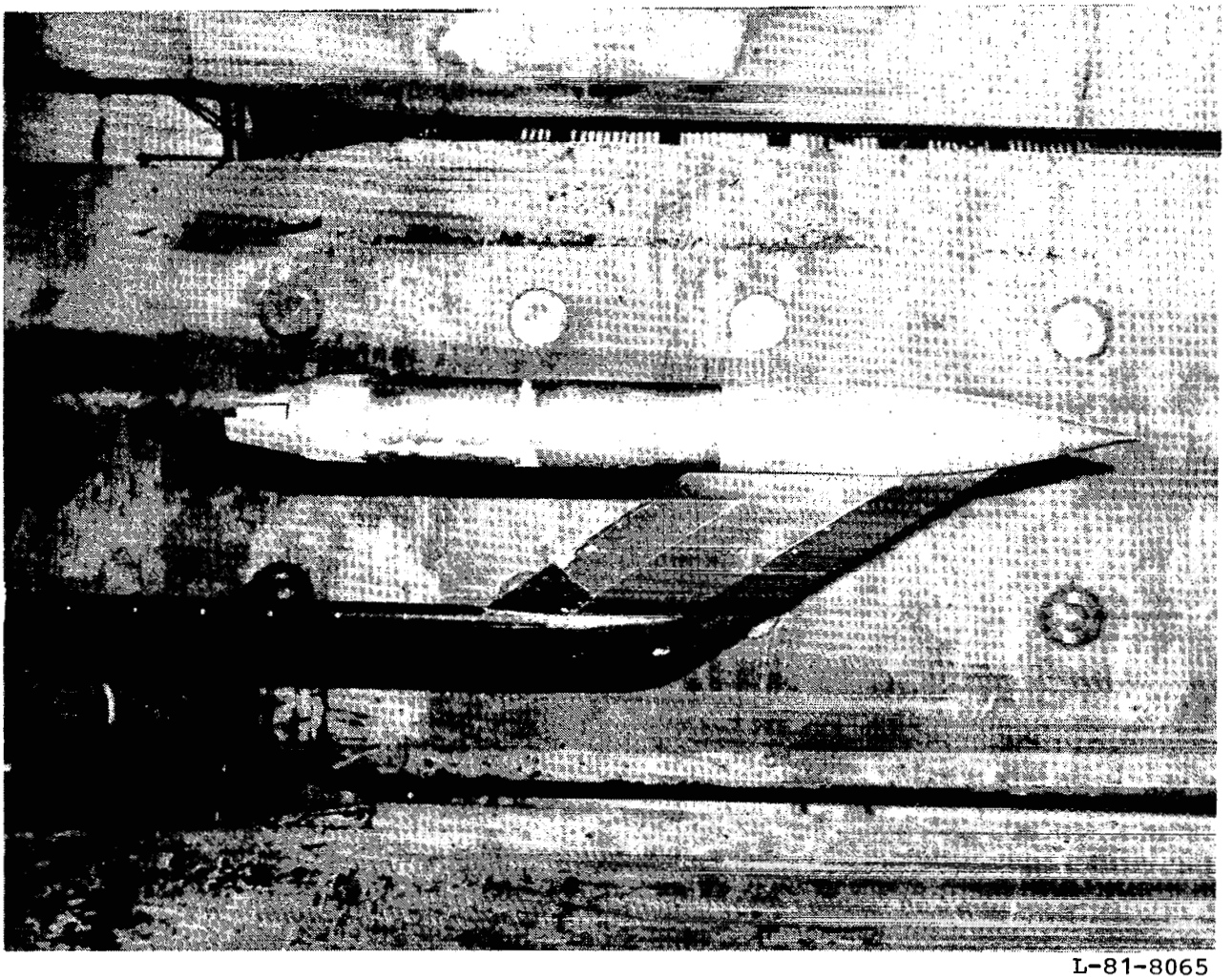

L-81-8065

(a) Langley 16-Foot Transonic Tunnel installation.

Figure 1.- Photographs of models and installations in test facilities.

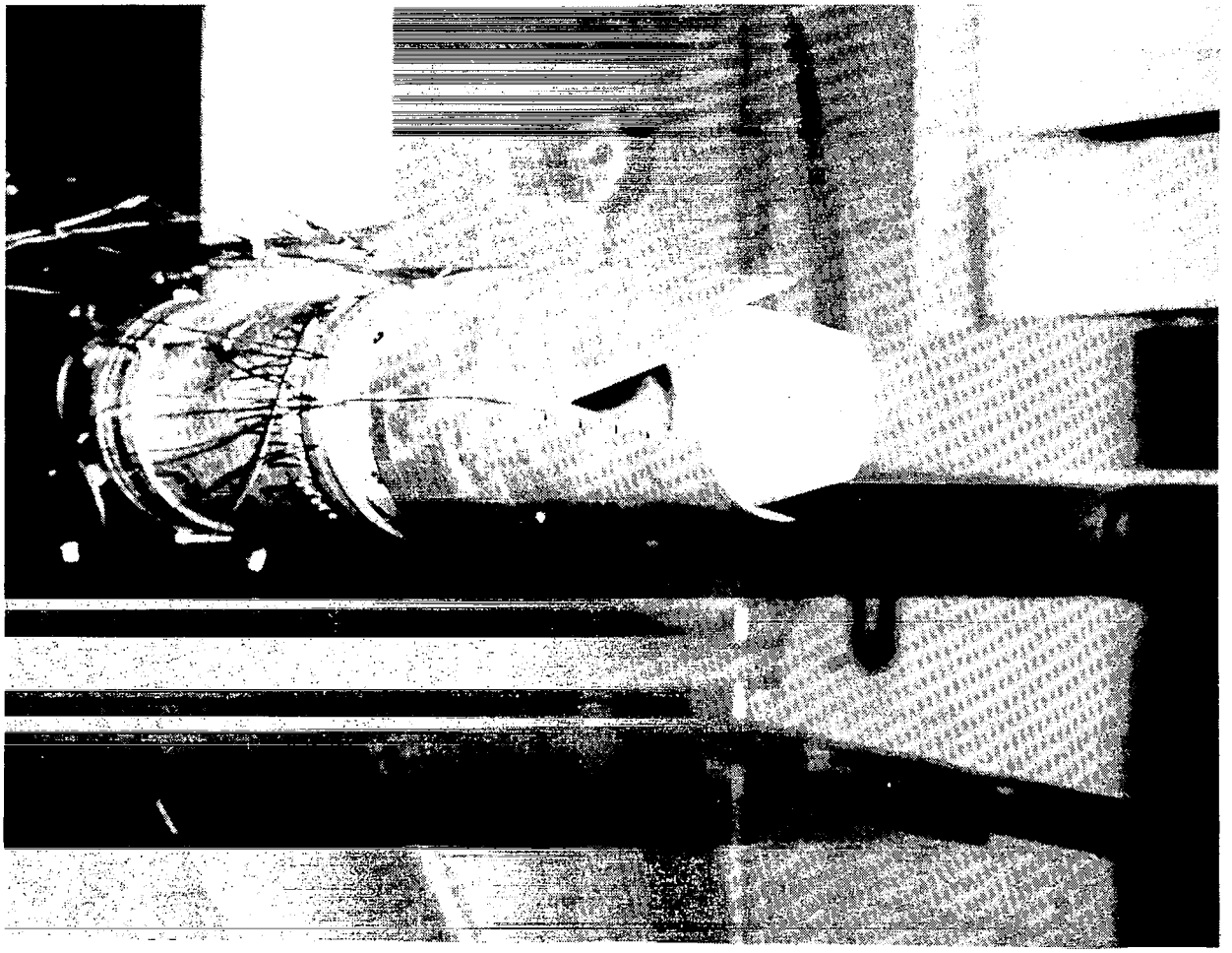

L-81-4188

(b) Static-test facility of 16-Foot Transonic Tunnel installation.

Figure 1.- Continued.

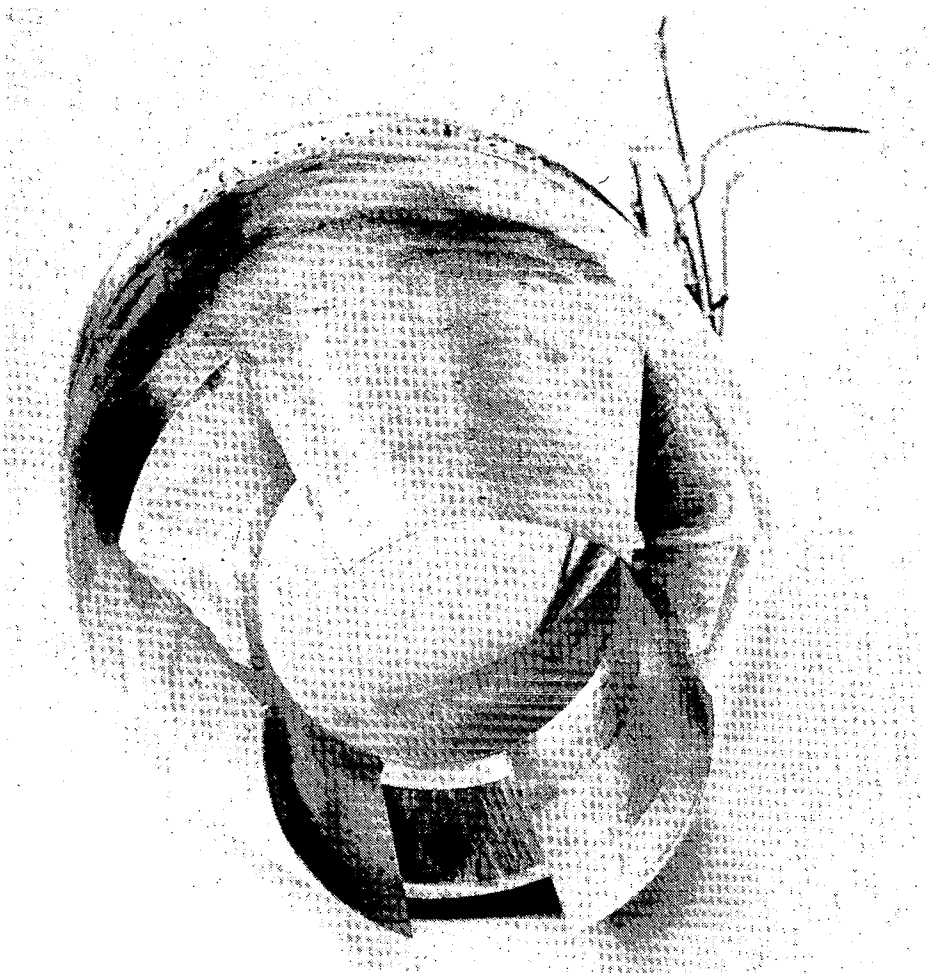

L-81-7699

(c) Low-expansion-ratio (A_e/A_t = 1.22) ventilated nozzle; configuration V-1.22.

Figure 1.- Continued.

L-81-7700

(d) High-expansion-ratio (A_e/A_t = 2.24) ventilated nozzle; configuration V-2.24.

Figure 1.- Concluded.

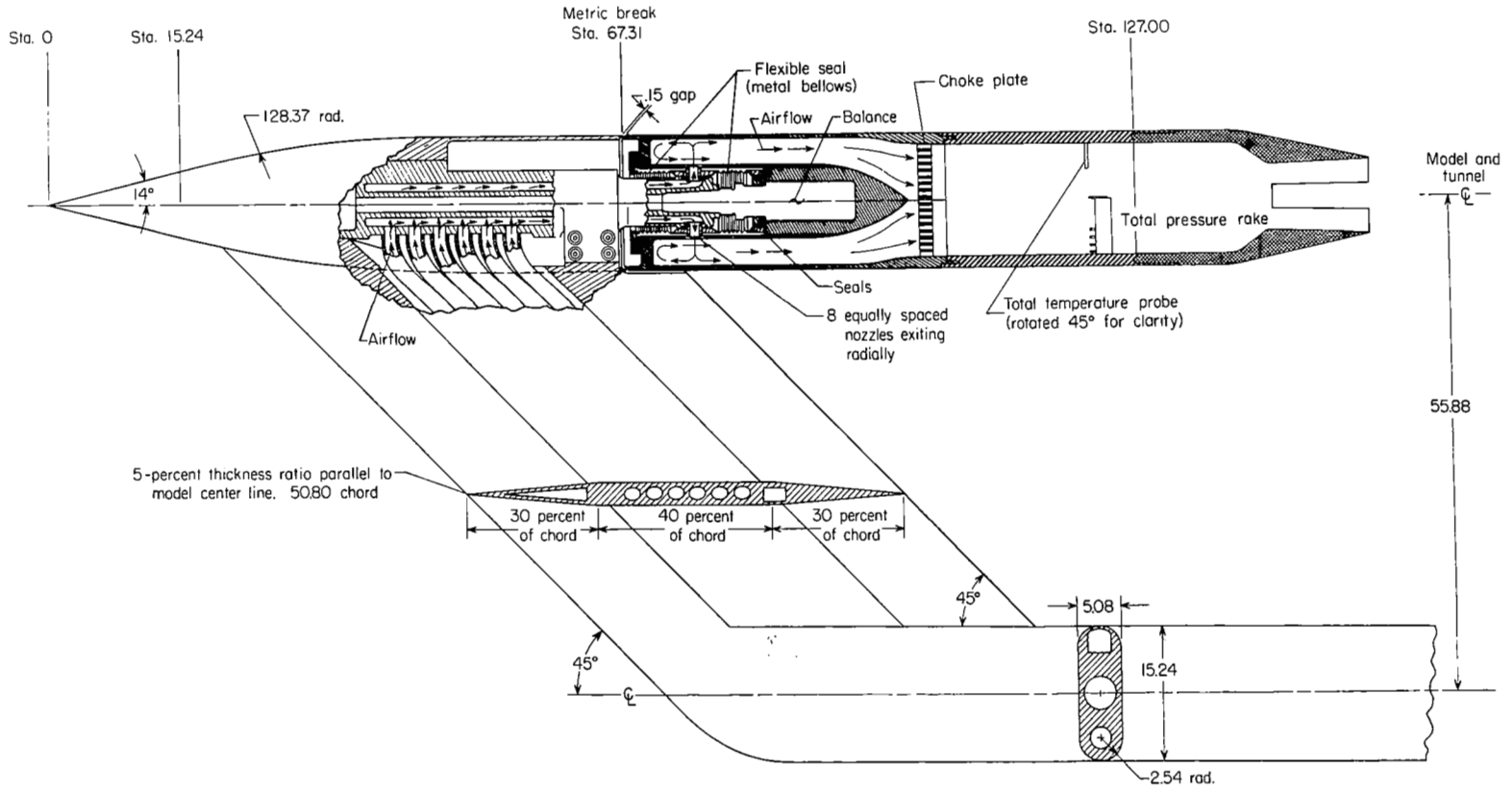

Figure 2.- Sketch showing general arrangement of air-powered single-engine nacelle model (16TT installation). All dimensions are in centimeters unless otherwise noted.

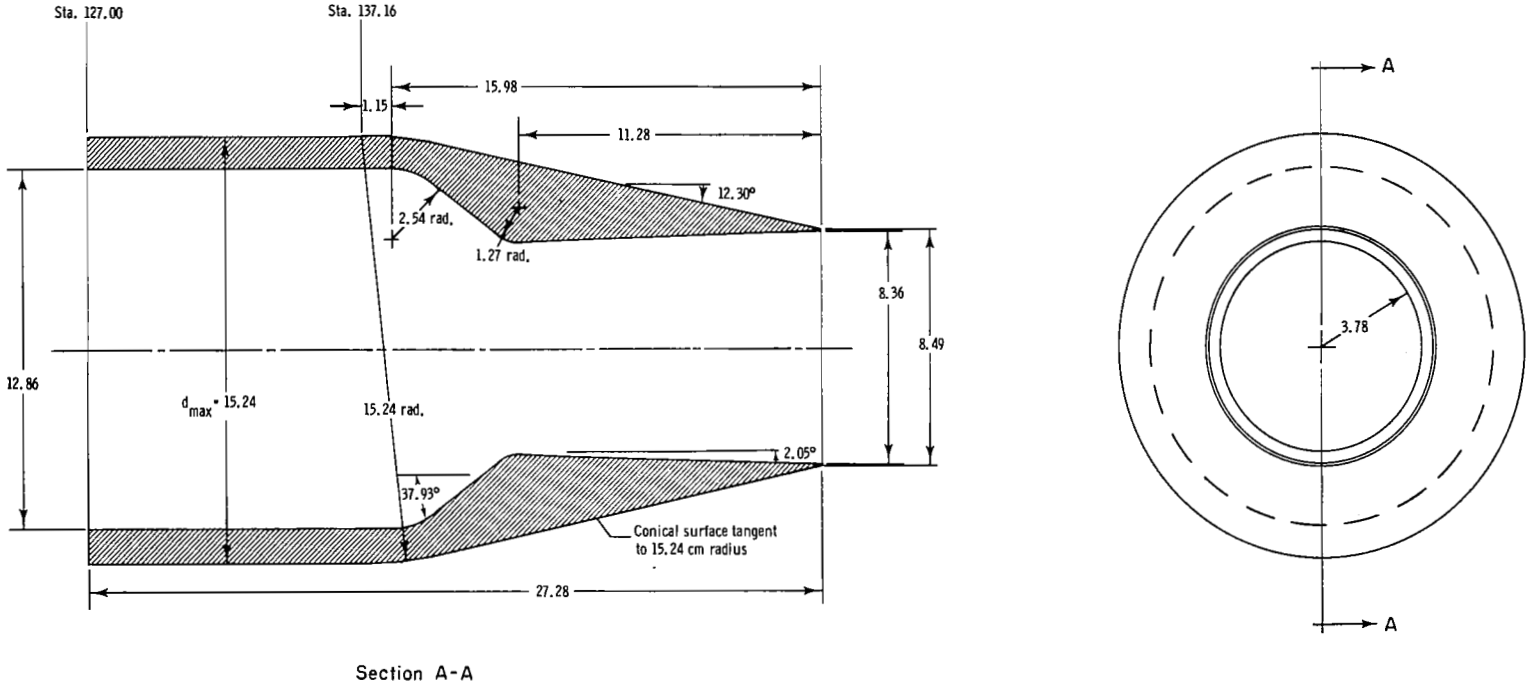

Section A-A

(a) Baseline low-expansion-ratio (A_e/A_t = 1.22) nozzle; configuration B-1.22.

Figure 3.- Sketches of baseline and ventilated nozzle hardware. All dimensions are in centimeters.

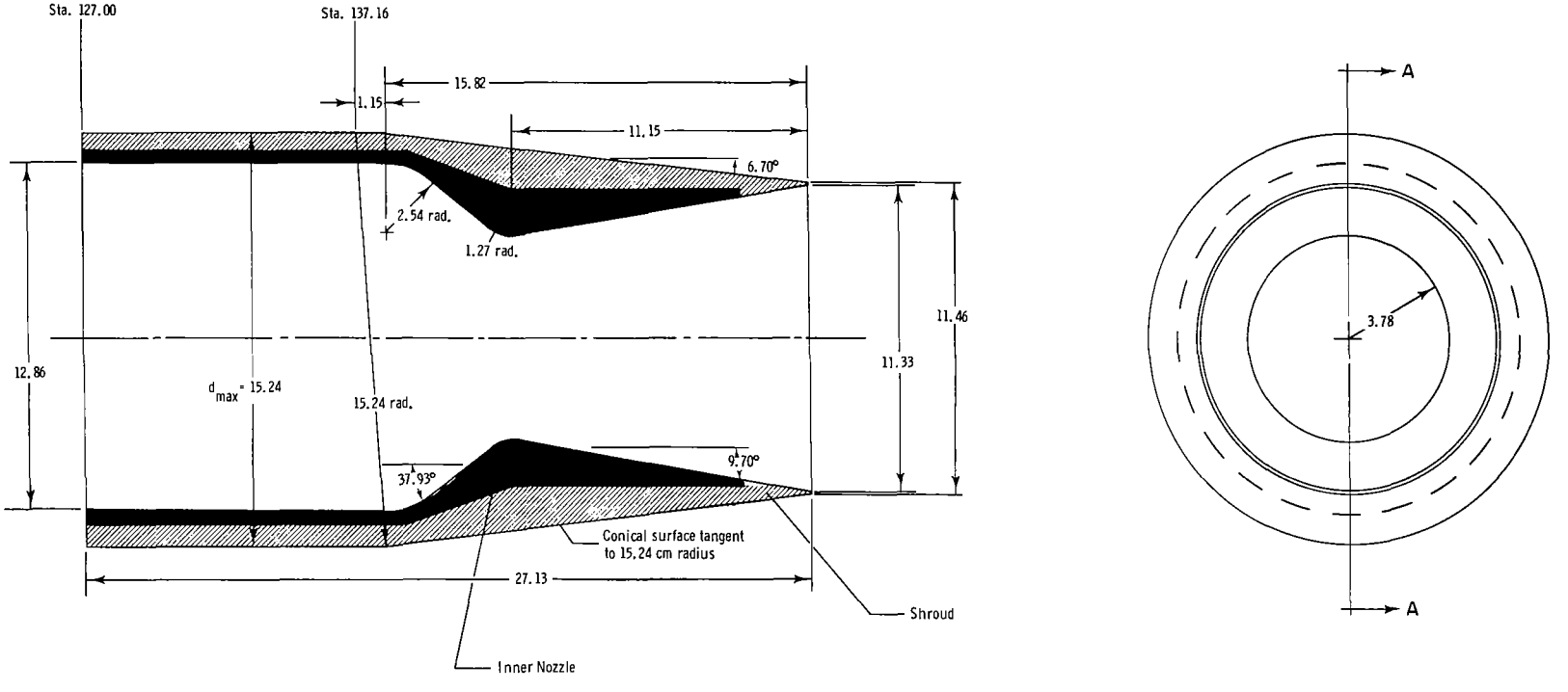

Section A-A

(b) Baseline high-expansion-ratio (A_e/A_t = 2.24) nozzle; configuration B-2.24.

Figure 3.- Continued.

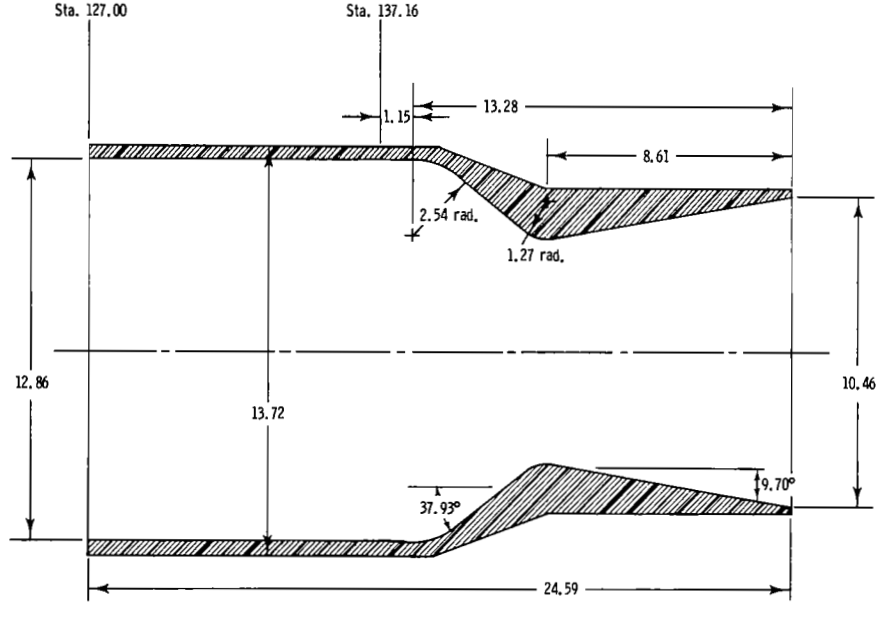

Section A-A

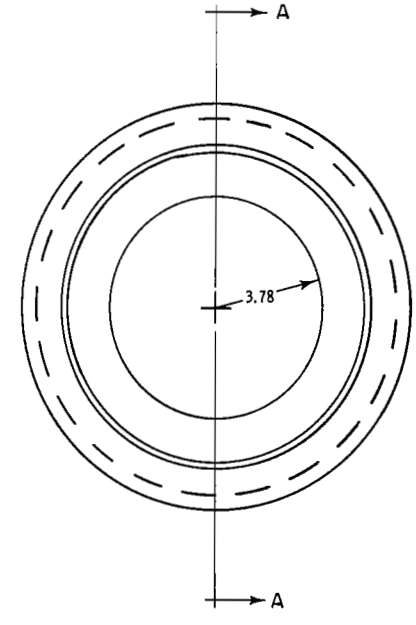

(c) Baseline intermediate-expansion-ratio (A_e/A_t = 1.91) nozzle; configuration B-1.91.

Figure 3.- Continued.

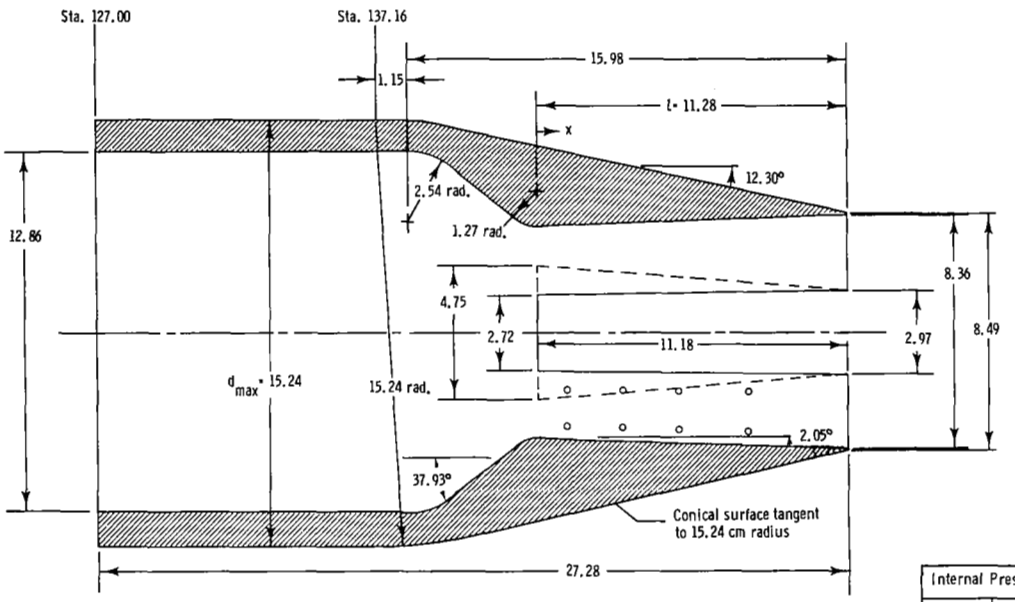

Section A-A

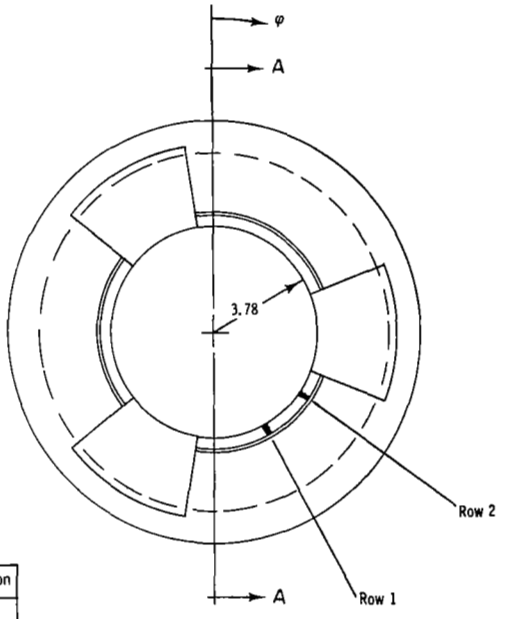

Internal Pressure Instrumentation		
	φ	x/l
Row 1	129.1°	.090
	129.1°	.271
	129.1°	.452
	129.1°	.679
Row 2	121.5°	.090
	121.5°	.271
	121.5°	.452
	121.5°	.679

(d) Ventilated low-expansion-ratio (A_e/A_t = 1.22) nozzle; configuration V-1.22.

Figure 3.- Continued.

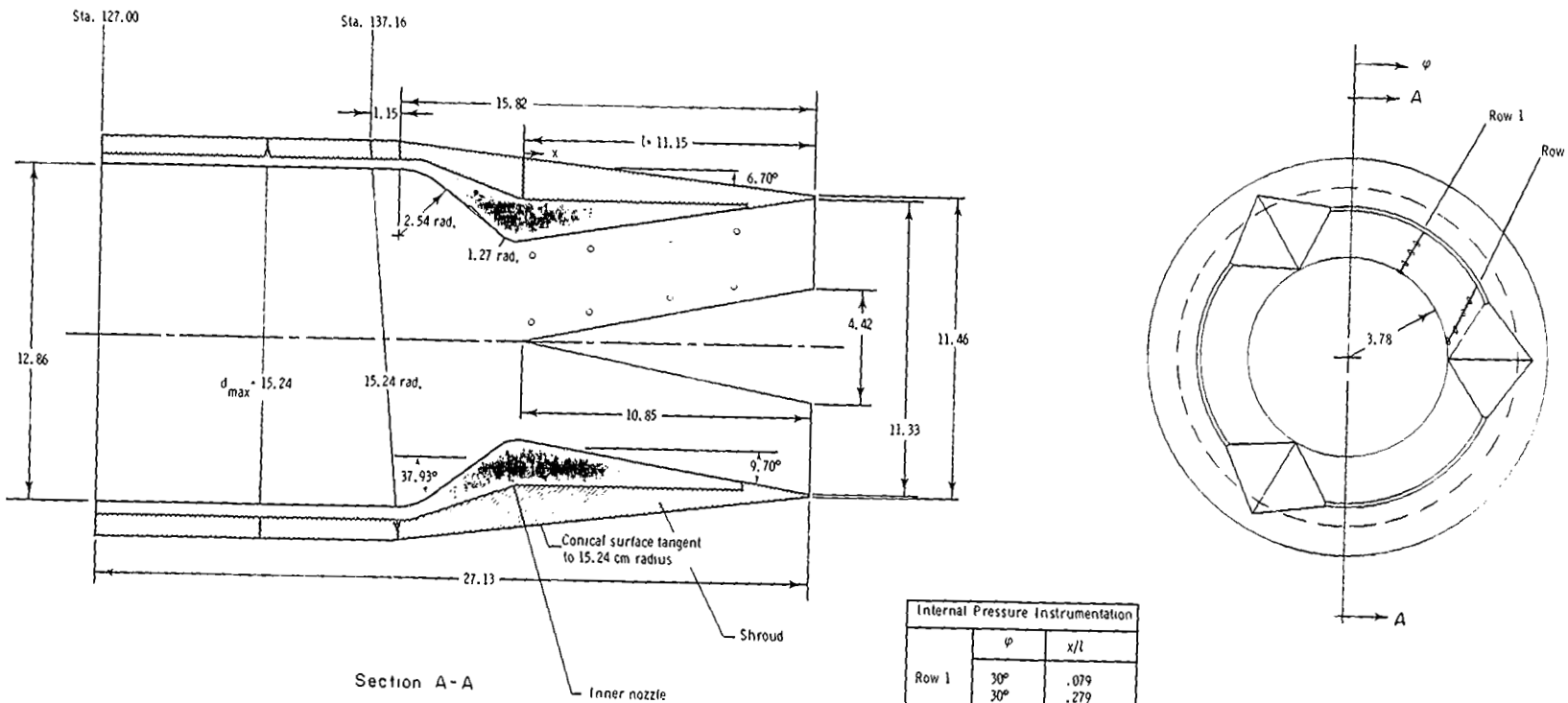

Internal Pressure Instrumentation		
	φ	x/l
Row 1	30°	.079
	30°	.279
	30°	.510
	30°	.737
Row 2	78°	.079
	72.5°	.279
	66°	.510
	62°	.728

(e) Ventilated high-expansion-ratio (A_e/A_t = 2.24) nozzle; configuration V-2.24.

Figure 3.- Continued.

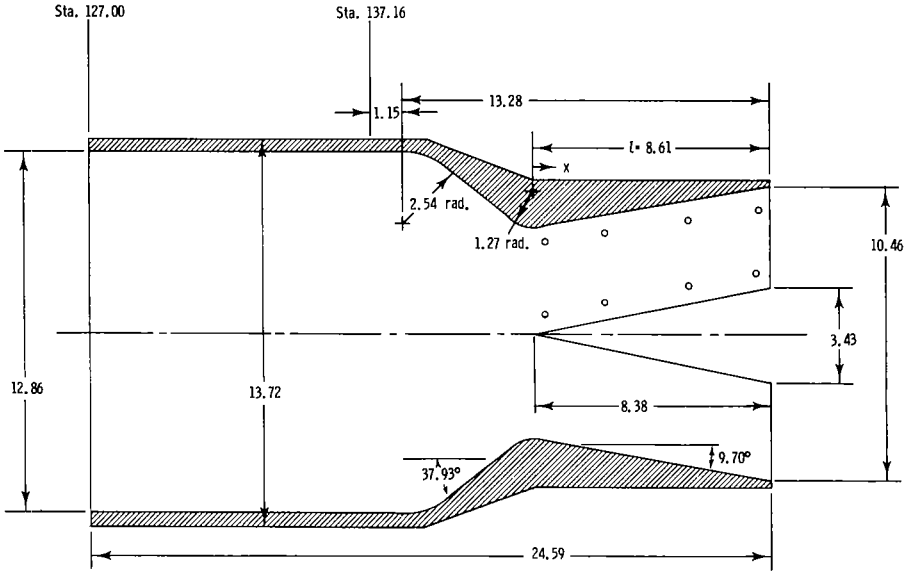

Section A-A

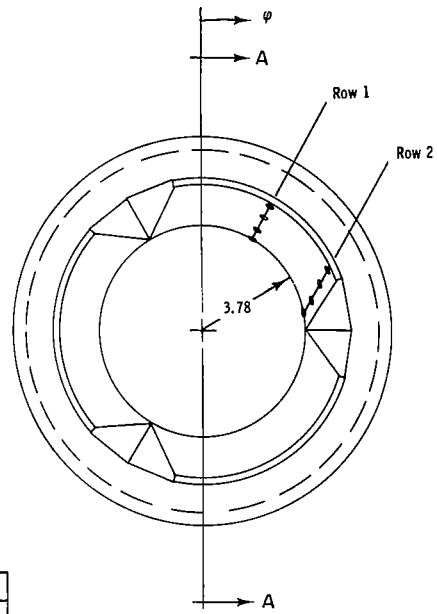

Internal Pressure Instrumentation		
	φ	x/l
Row 1	29°	.103
	29°	.361
	29°	.660
	29°	.953
Row 2	79.5°	.103
	74°	.361
	68.3°	.660
	64.5°	.941

(f) Ventilated intermediate-expansion-ratio (A_e/A_t = 1.91) nozzle; configuration V-1.91.

Figure 3.- Concluded.

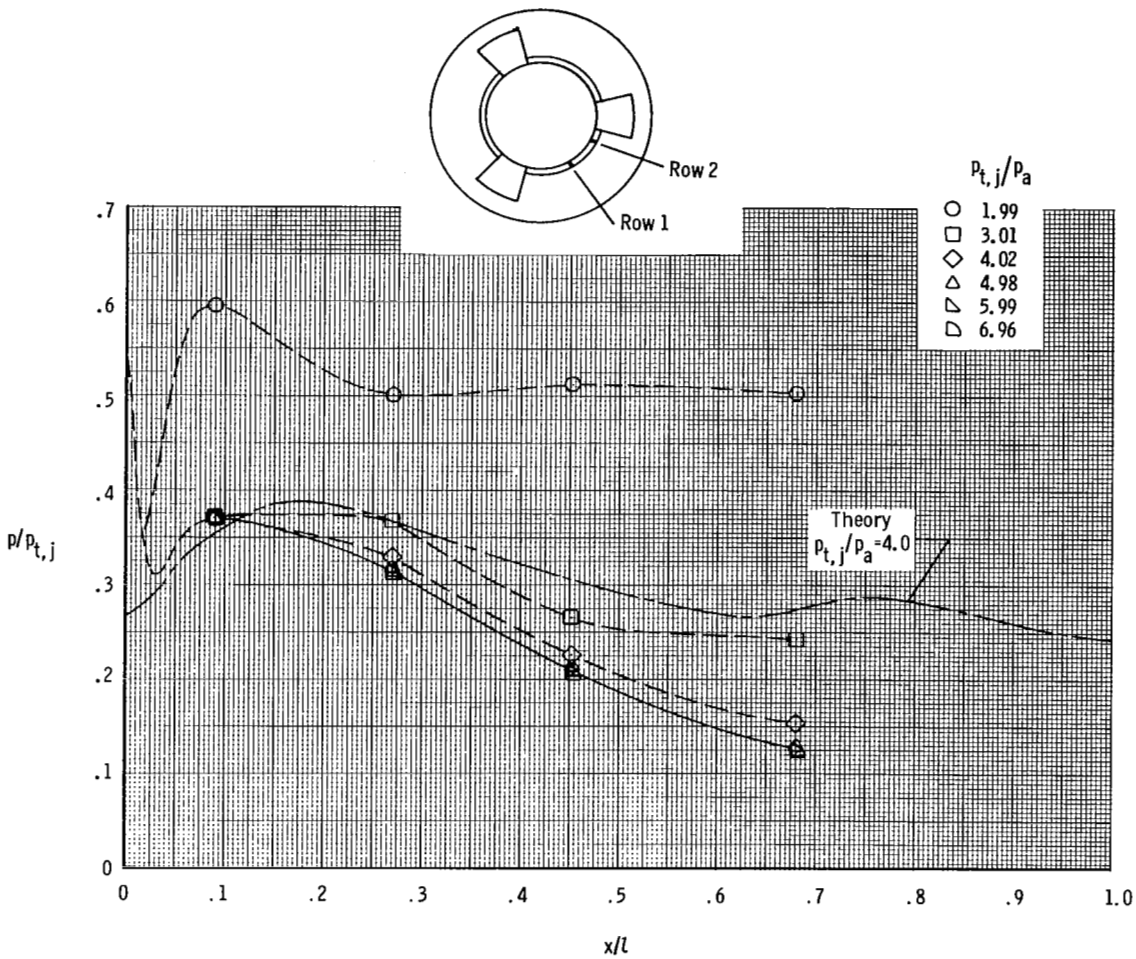

(a) Row 1.

Figure 4.- Nozzle internal static-pressure distributions for nozzle configuration V-1.22 at static conditions.

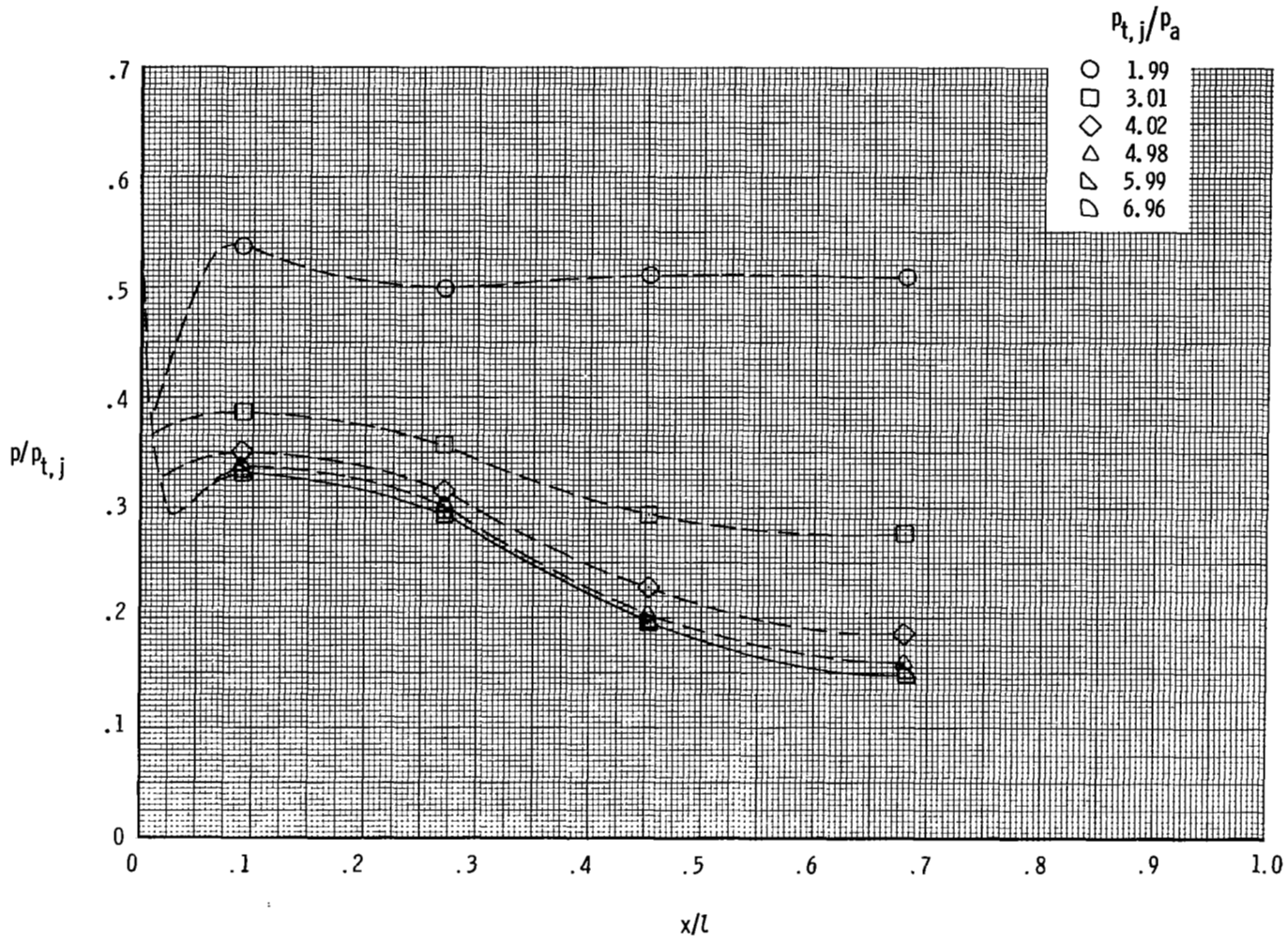

(b) Row 2.

Figure 4.- Concluded.

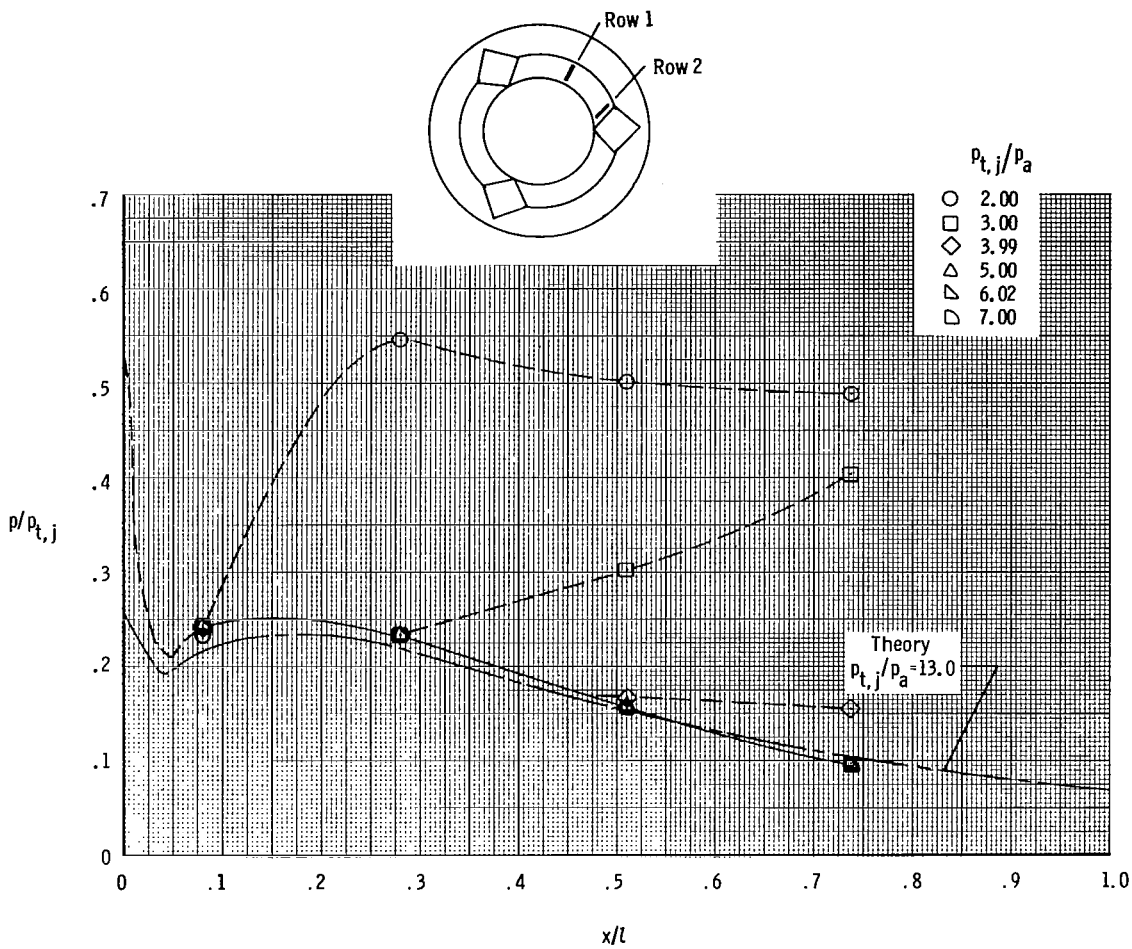

(a) Row 1.

Figure 5.- Nozzle internal static-pressure distributions for nozzle configuration V-2.24 at static conditions.

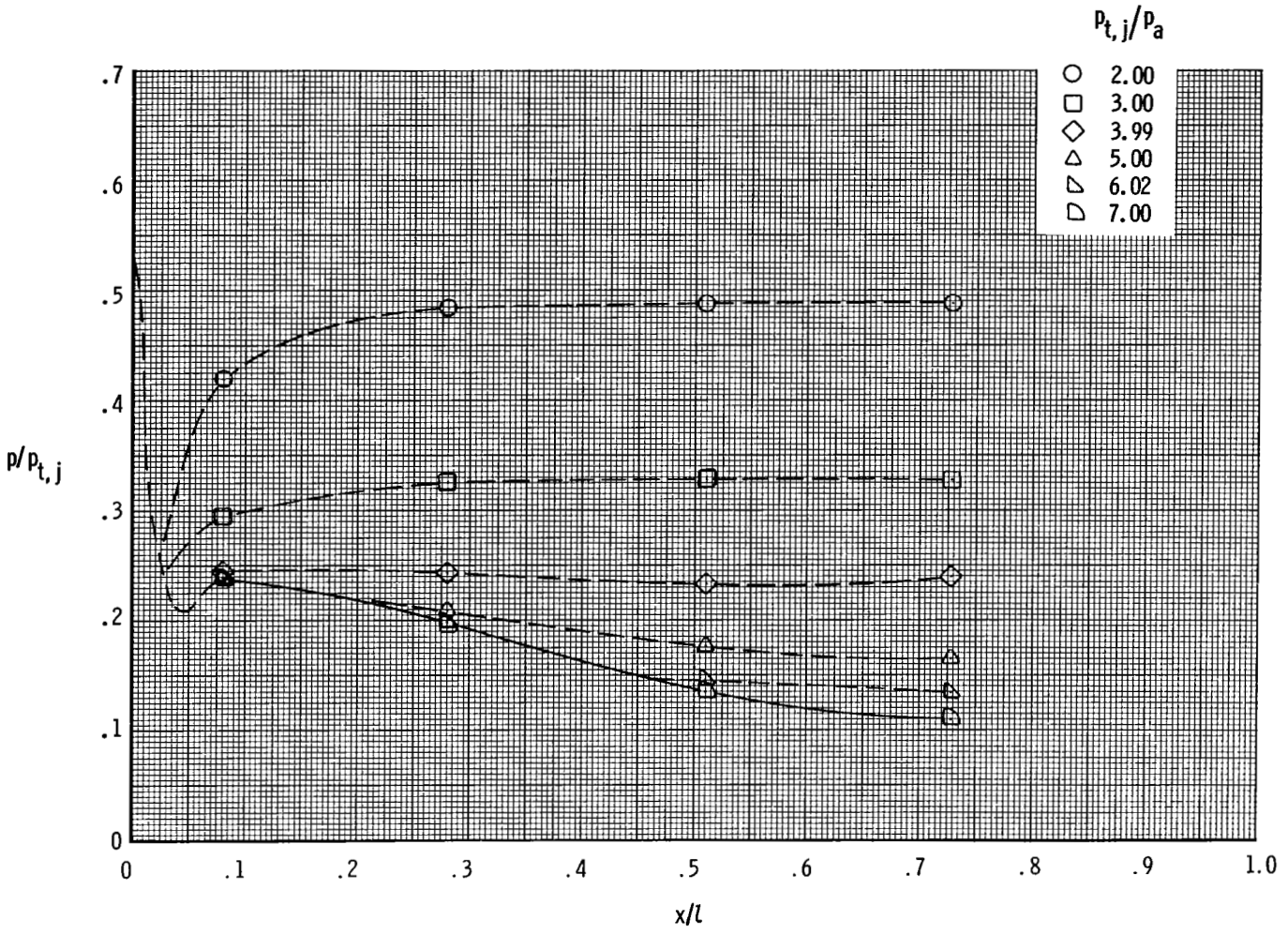

(b) Row 2.

Figure 5.- Concluded.

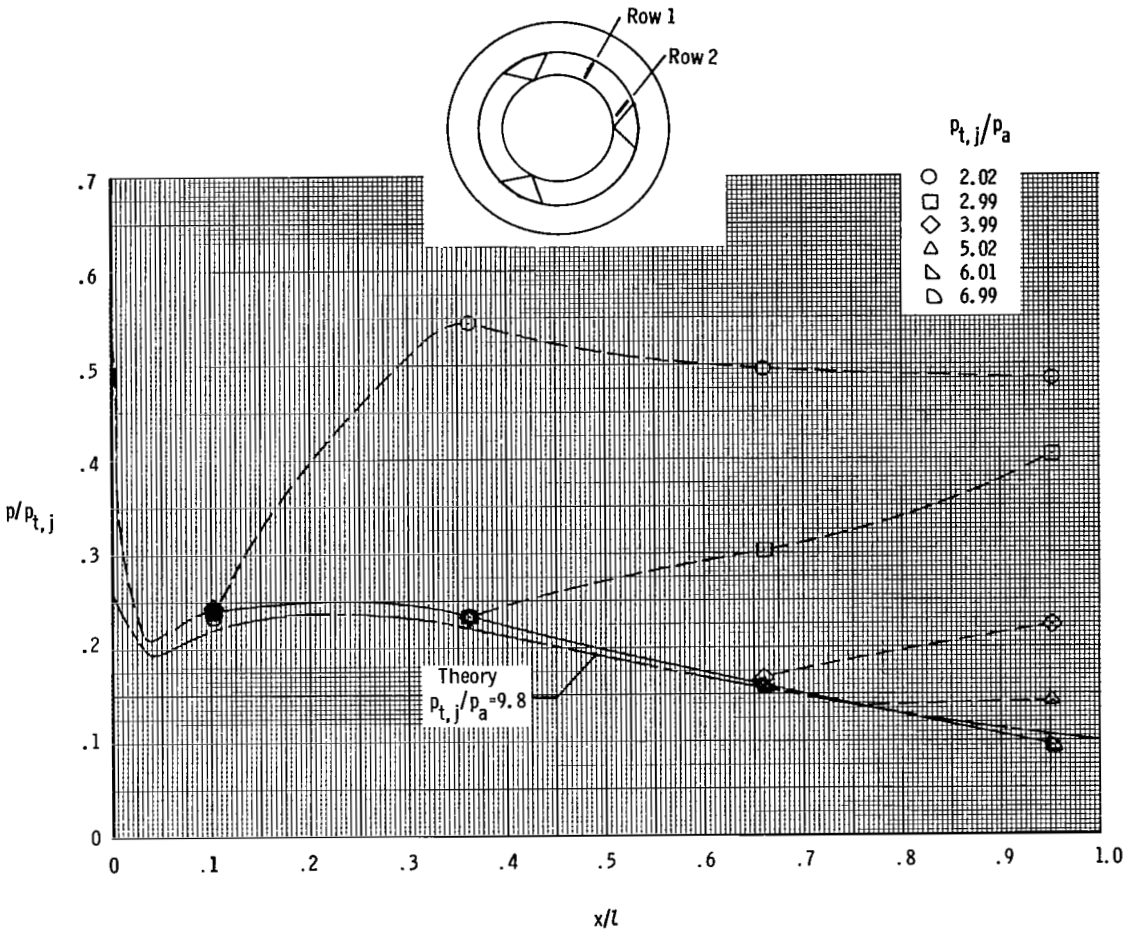

(a) Row 1.

Figure 6.- Nozzle internal static-pressure distributions for nozzle configuration V-1.91 at static conditions.

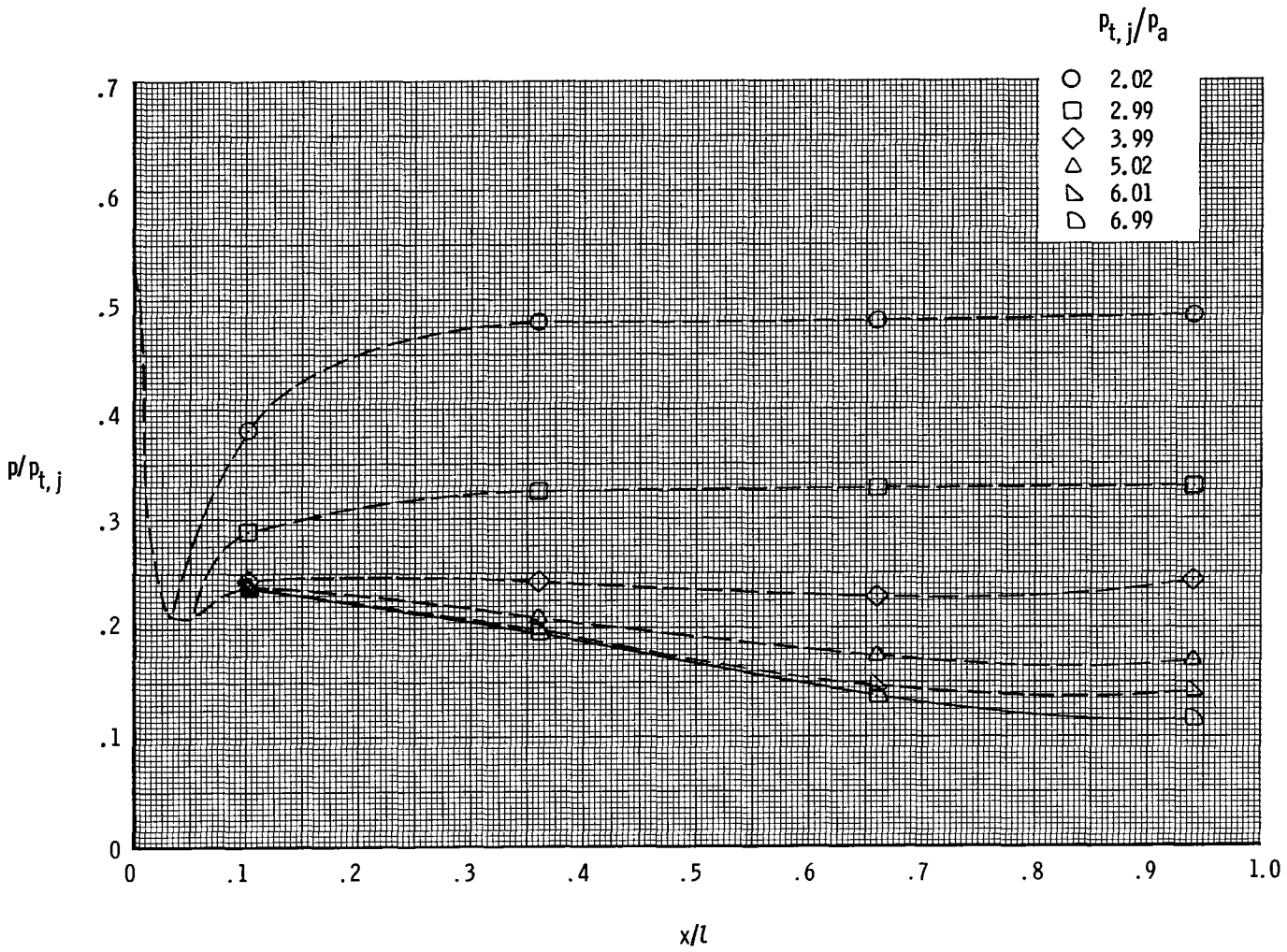

(b) Row 2.

Figure 6.- Concluded.

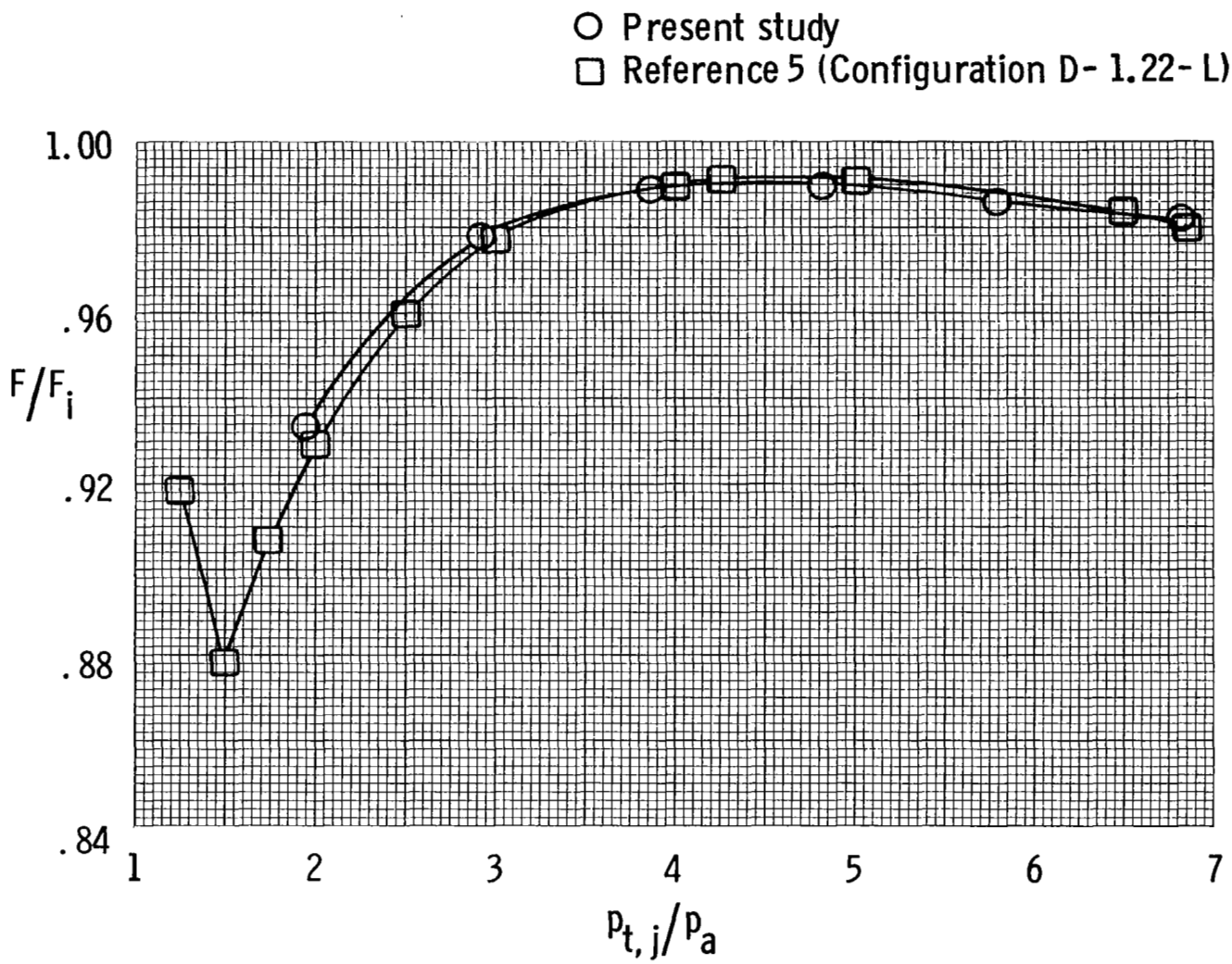

(a) Baseline nozzle configuration B-1.22.

Figure 7.- Comparison of static thrust ratios for present study with previous investigation (ref. 5).

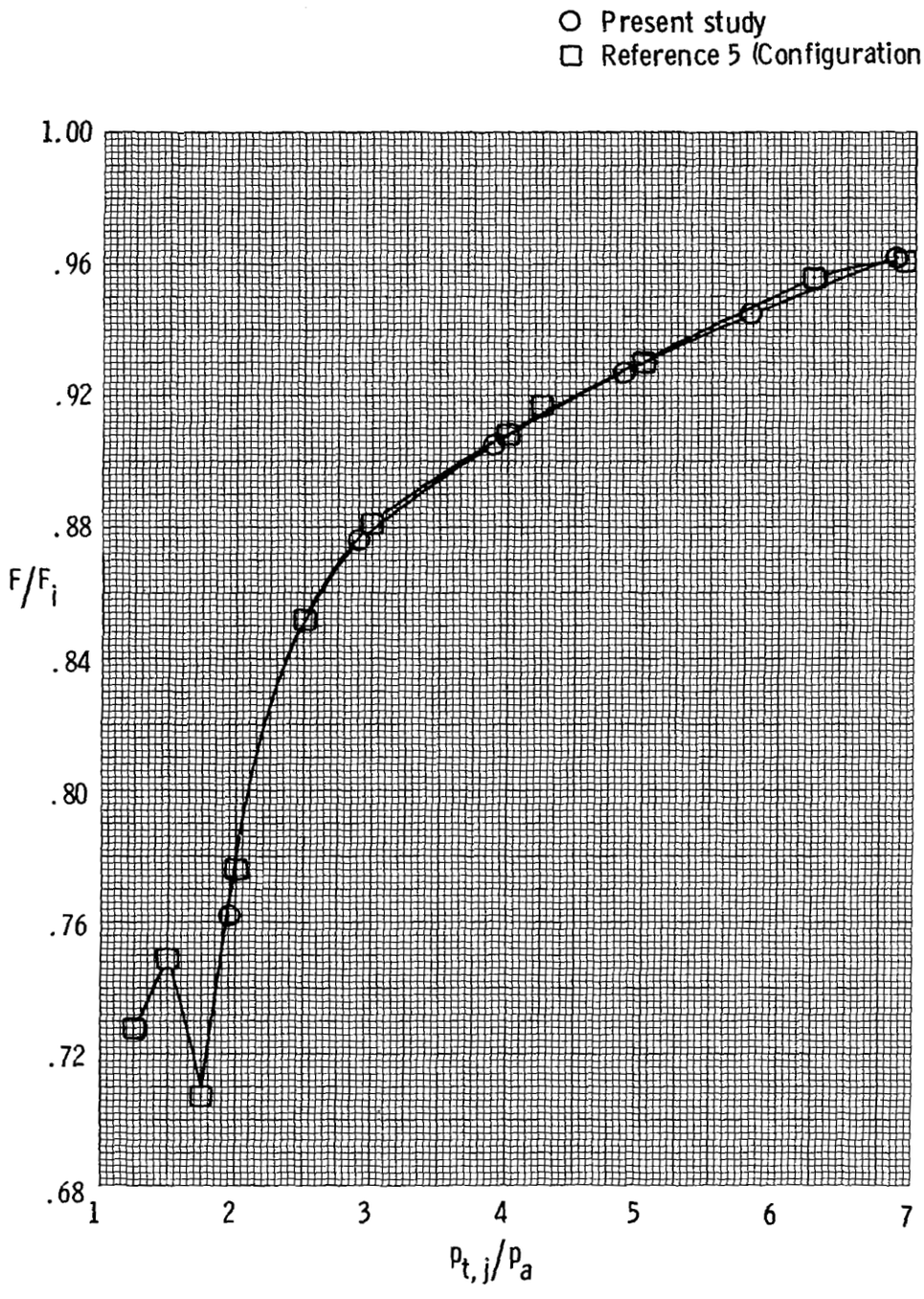

(b) Baseline nozzle configuration B-2.24.

Figure 7.- Concluded.

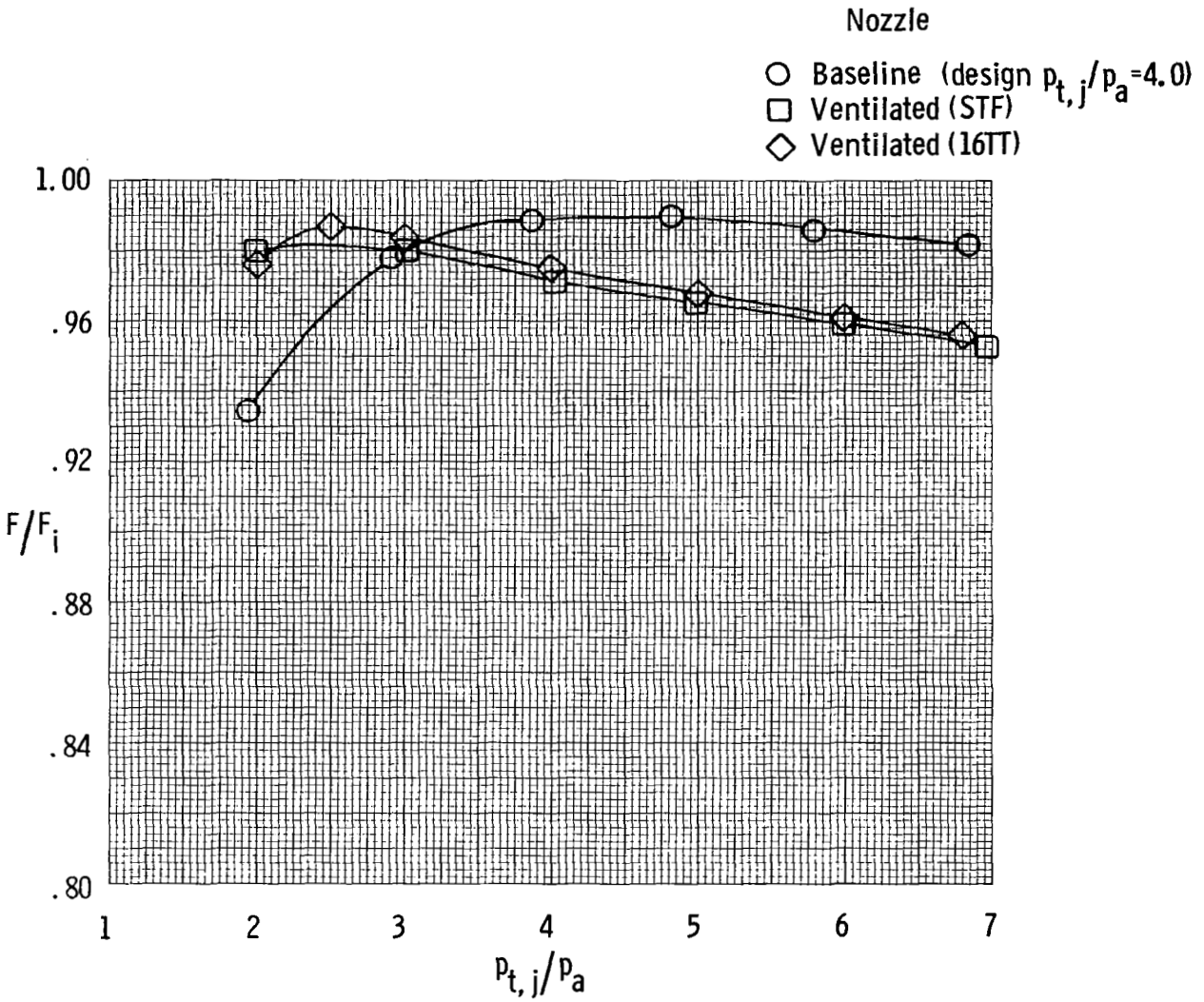

(a) Low-expansion-ratio nozzle (A_e/A_t = 1.22).

Figure 8.- Variation of thrust ratio at static conditions.

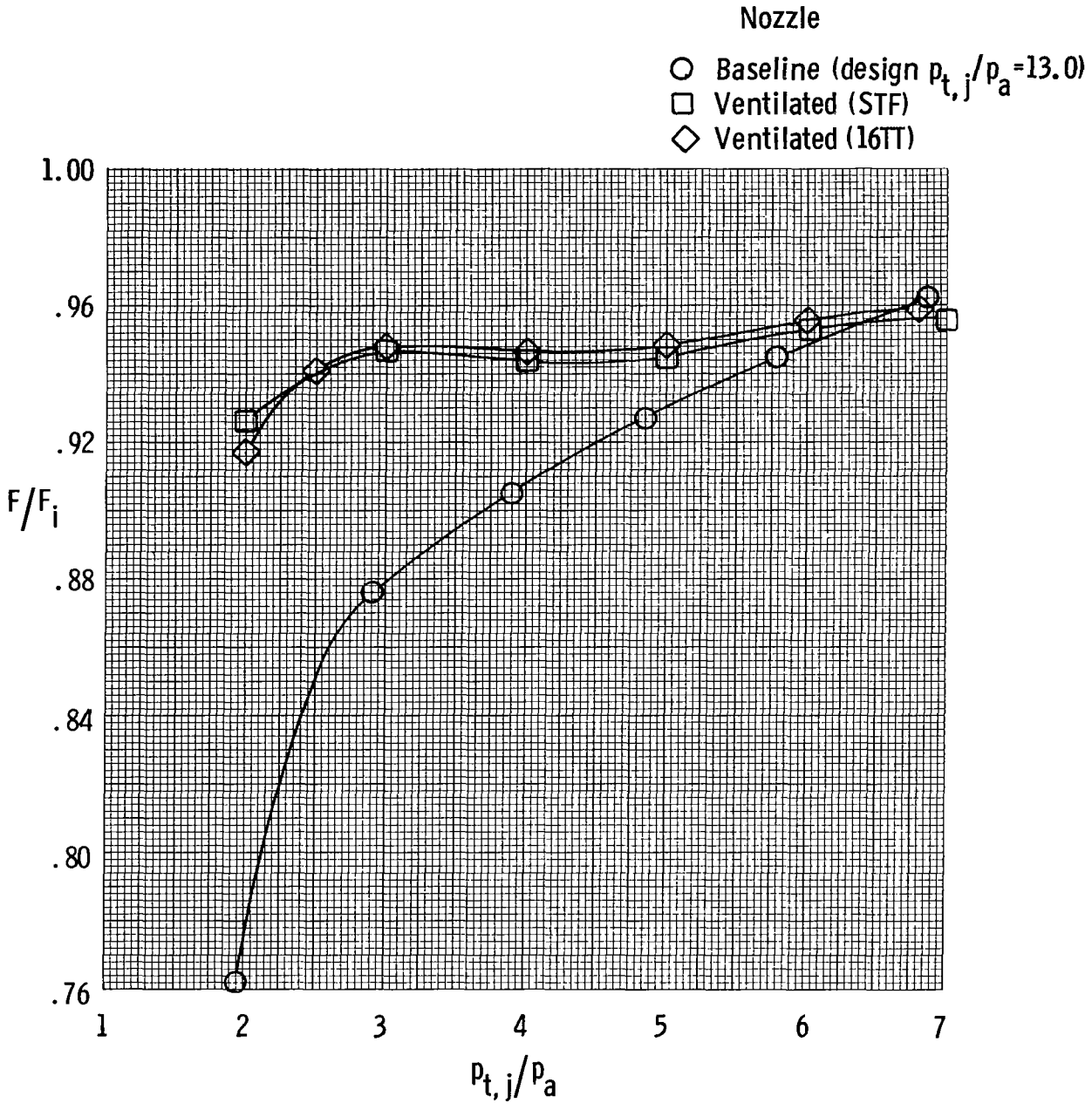

(b) High-expansion-ratio nozzle (A_e/A_t = 2.24).

Figure 8.- Continued.

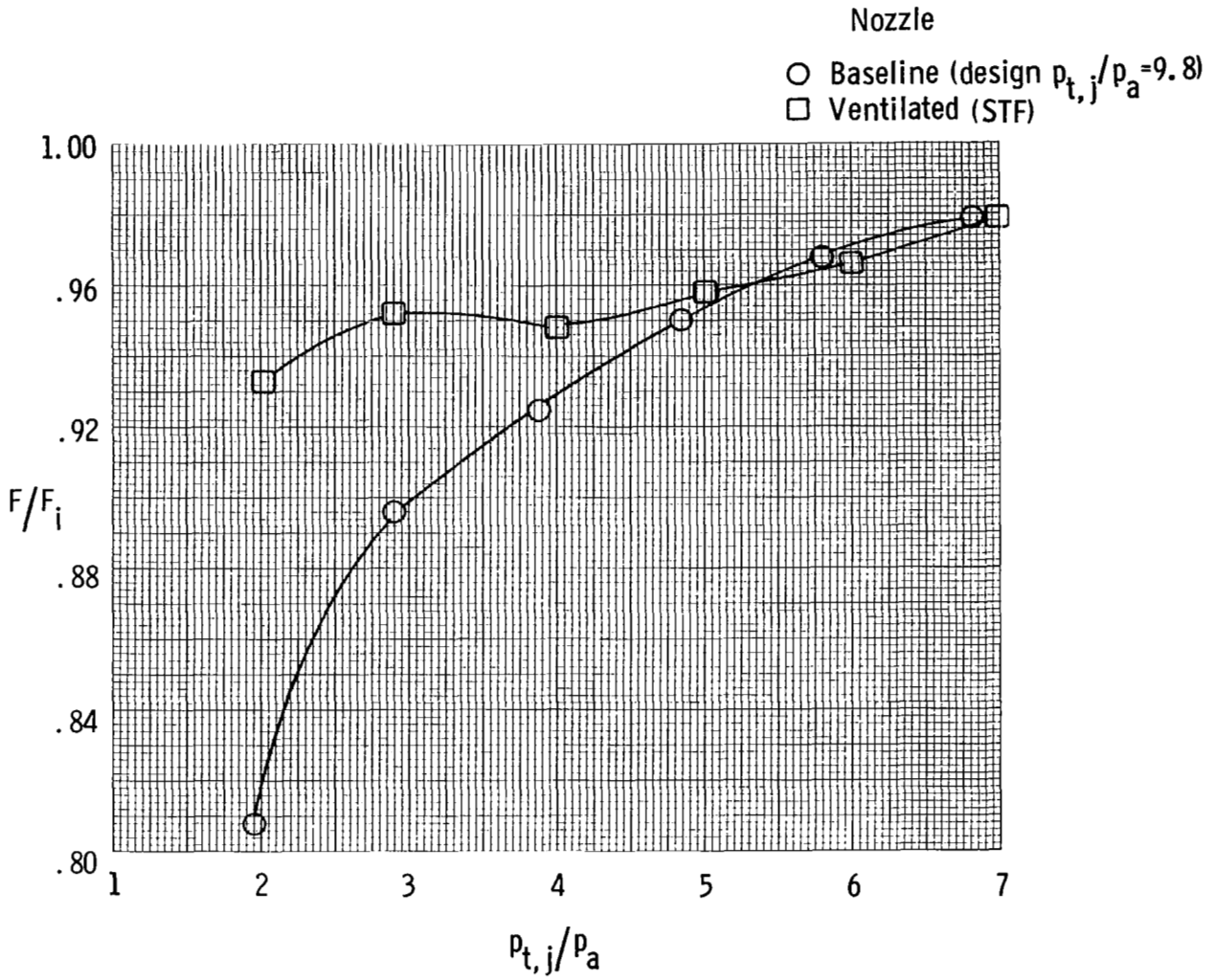

(c) Intermediate-expansion-ratio nozzle (A_e/A_t = 1.91).

Figure 8.- Concluded.

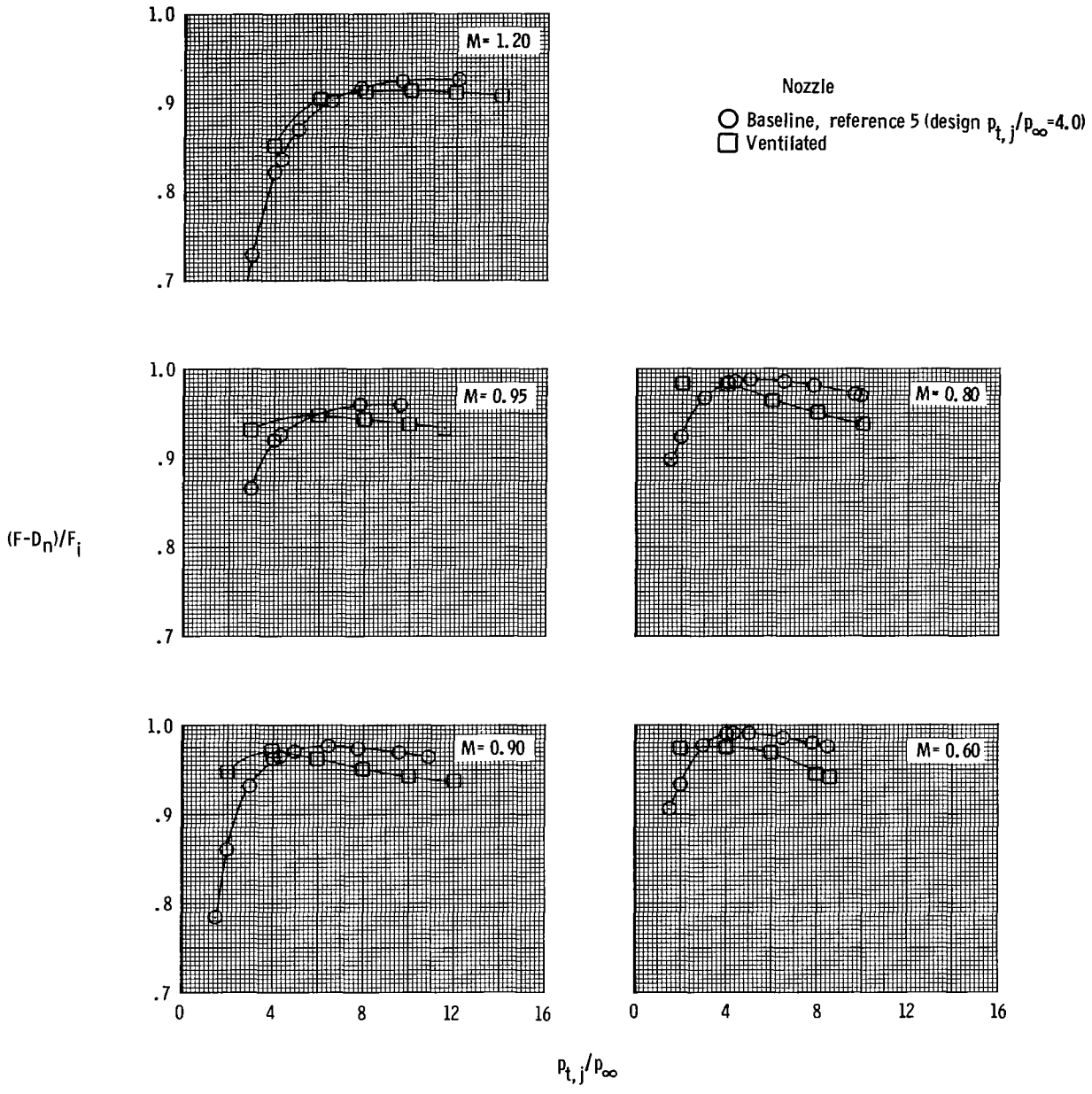

(a) Low-expansion-ratio nozzle (A_e/A_t = 1.22).

Figure 9.- Variation of thrust-minus-drag ratio with jet total pressure ratio at several test Mach numbers.

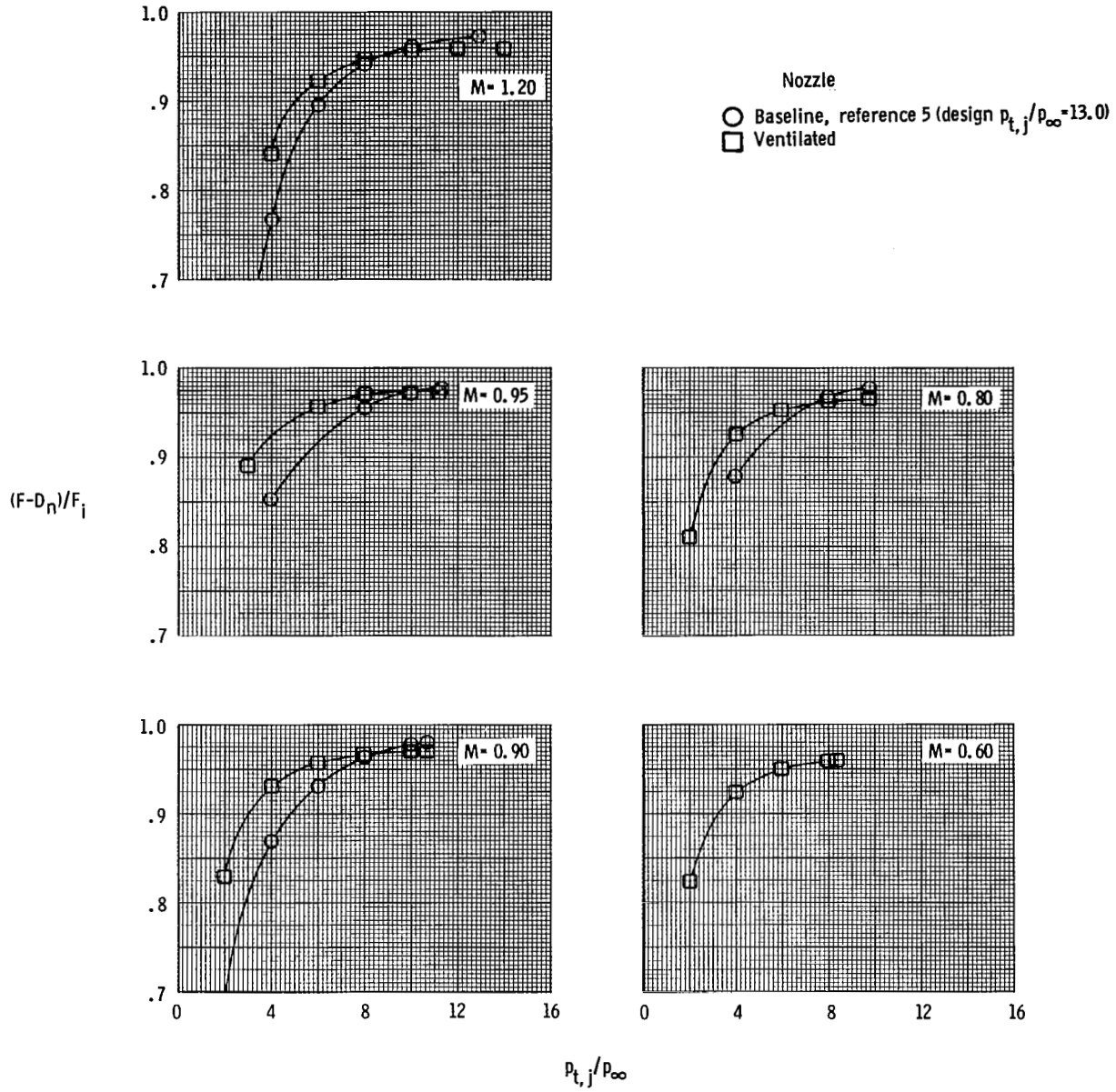

(b) High-expansion-ratio nozzle (A_e/A_t = 2.24).

Figure 9.- Concluded.

1. Report No.	2. Government Accession No.	3. Recipient's Catalog No.
NASA TP-2013		

4. Title and Subtitle	5. Report Date
PERFORMANCE CHARACTERISTICS OF AXISYMMETRIC CONVERGENT-DIVERGENT EXHAUST NOZZLES WITH LONGITUDINAL SLOTS IN THE DIVERGENT FLAPS	June 1982
	6. Performing Organization Code: 505-43-23-01
7. Author(s): Laurence D. Leavitt and Linda S. Bangert	8. Performing Organization Report No.: L-15119
	10. Work Unit No.
9. Performing Organization Name and Address: NASA Langley Research Center, Hampton, VA 23665	11. Contract or Grant No.
	13. Type of Report and Period Covered: Technical Paper
12. Sponsoring Agency Name and Address: National Aeronautics and Space Administration, Washington, DC 20546	14. Sponsoring Agency Code

15. Supplementary Notes

16. Abstract

An investigation has been conducted in the Langley 16-Foot Transonic Tunnel and in the static-test facility of that tunnel to determine the effects of divergent flap ventilation of an axisymmetric nozzle on nozzle internal (static) and wind-on performance. Tests were conducted at 0° angle of attack at static conditions and at Mach numbers from 0.6 to 1.2. Ratios of jet total pressure to free-stream static pressure were varied from 1.0 (jet off) to approximately 14.0 depending on Mach number. The results of this study indicate that divergent flap ventilation generally provided large performance benefits at overexpanded nozzle conditions and performance reductions at underexpanded nozzle conditions when compared to the baseline (unventilated) nozzles. Ventilation also reduced the peak static and wind-on performance levels.

17. Key Words (Suggested by Author(s))	18. Distribution Statement
Convergent-divergent exhaust nozzles Longitudinal slots in divergent flaps Axisymmetric nozzles	Unclassified - Unlimited Subject Category 02

19. Security Classif. (of this report)	20. Security Classif. (of this page)	21. No. of Pages	22. Price
Unclassified	Unclassified	34	A03

For sale by the National Technical Information Service, Springfield, Virginia 22161

NASA-Langley, 1982